An Improved Robot Calibration Approach Based on Axis-Invariant

Ju Yiran[1,*]
[1]Department of Electrical and Computer Engineering, University of British Columbia,
V6T 1Z4 Vancouver, Canada
Email: juyiran@alumni.ubc.ca

Meng Yu[2]
[2]College of Astronautics, Nanjing University of Aeronautics and Astronautics
Nanjing, China
Email：yuxy21@nuaa.edu.cn

***Abstract*— In this paper, we introduce an enhanced method for measuring robot structural parameters leveraging Axis Invariants. We begin by redefining fixed-axis rotation and delving into axis invariants. Using a laser tracker, we measure the positions of two tracking balls affixed to the robot end to determine joint axis directions, positions, and angular positions or linear positions based on the fixed-axis rotation concept. Subsequently, these findings are employed to ascertain the robot's DH parameters. Both theoretical analysis and experimental validation demonstrate the efficacy of our proposed principle, which notably enhances the robot's absolute positioning accuracy. A salient advantage of this principle is its ability to measure structural parameters without necessitating communication with the robot, thereby simplifying the measurement process.**

Keywords*— *calibration, axis invariant, positioning accuracy, robot, laser tracker

I. INTRODUCTION

Absolute position accuracy of manipulators is crucial in industrial applications. While manipulators often boast high repetitive positioning precision, their absolute accuracy leaves much to be desired—a factor pivotal to offline programming. The primary source of error affecting the accuracy of industrial robots is the geometrical parameter error [1,2]. Such errors primarily stem from manufacturing tolerances and assembly deviations[3,4]. Given that these geometric errors can result in significant orientation discrepancies of the end effector, it is imperative to address and rectify them.

Much work has been done on the calibration of manipulators[5–10], most of which are based on distance constraints. Robot calibration is considered as an effective method to eliminate or reduce geometric errors, thus improving the absolute precision of robots. In general, classical calibration procedures are divided into four steps: Modeling, Measurement, Identification, and Verification and Correction. At present, there exist various calibration techniques that are able to calibrate geometric model of manipulators by using different modelling, measurement and identification methods [11–13]. The focus of modelling is to develop a proper kinematic model to describe the relationship between joint positions and posture of the end effector, and the model should be complete, minimal, and continuous[14]. Chen[15] proposed a zero reference exponential product model, which aims to create a coordinate system for the base and the end of the robot, and represents each joint with displacement rotation, and there is no need to establish corresponding coordinate systems for each joint. Ish[16] identified sources of absolute errors, and discussed methods of creating kinematic models and robot calibration. Ha[17] calibrated the robot using the relative position, without calibrating transformation from the world coordinate system to the robot base coordinate system. A lot of research has been done on measurement methods[18–22], and various measuring instruments are also effective. With the continuous progress of technology, more and more new measurement technologies will be proposed. Meng and Zhuang[23] presented a vision-based self-calibration method for a serial manipulator. Du[24] presented an online robot self-calibration method based on an inertial measurement unit and a position sensor, and used Kalman filter to estimate the position and direction of a manipulator. Parameter identification is based on the error model of the robot End-effector to identify and calculate the actual values of the parameters affecting the precision of End-effector[25–28]. Dolinsky[29] introduced a new inverse static kinematic calibration technique based on genetic programming to establish and identify model structure and parameters.

P. Xiao[30] introduced a method for measuring robot structural parameters using axis invariants. However, this approach didn't account for joint angle positions and required communication with the robot. This paper presents an enhanced methodology based on axis invariants. We redefine fixed-axis rotation, employ a laser tracker to gauge the positions of two tracking balls on the robot end, and use this data to determine joint axis directions, positions, and angle or line positions. These measurements then inform the robot's DH parameters. Our analysis and experiments validate this improved approach, highlighting its capability to enhance the robot's absolute positioning accuracy.

II. NOTATIONS

Given by 3D coordinate vectors $a = \left[a^{[1]}, a^{[2]}, a^{[3]}\right]$, $b = \left[b^{[1]}, b^{[2]}, b^{[3]}\right]$, one has

$$\tilde{a}\cdot\tilde{b} = b\cdot a^{\mathrm{T}} - a^{\mathrm{T}}\cdot b\cdot \mathbf{1} \tag{1}$$

$$\widetilde{\tilde{a}\cdot b} = b\cdot a^{\mathrm{T}} - a\cdot b^{\mathrm{T}} \tag{2}$$

where the **coordinate vector defaults to a column vector** and

$$\tilde{a} = \begin{bmatrix} 0 & -a^{[3]} & a^{[2]} \\ a^{[3]} & 0 & -a^{[1]} \\ -a^{[2]} & a^{[1]} & 0 \end{bmatrix} \tag{3}$$

The specification of the structural parameters of the robot arm is shown in Fig.1. The **r**adial position coordinate vector from the **origin** of Frame# i to a point P attached to Frame#6 is noted as ${}^{i}r_{6\mathrm{P}}$. The joint axis coordinate vector i.e., the direction vectors, between Frame#5 and Frame#6 are expressed as ${}^{5}n_{6}$, which are aligned with the **d**esired position ${}^{i}_{d}r_{6\mathrm{P}}$ and desired direction ${}^{i|5}_{d}n_{6}$, respectively by controlling the joint positions. ${}^{i}\boldsymbol{R}_{6}$ indicates that the kinematic chain is composed of 6 **R**evolute joint axes.

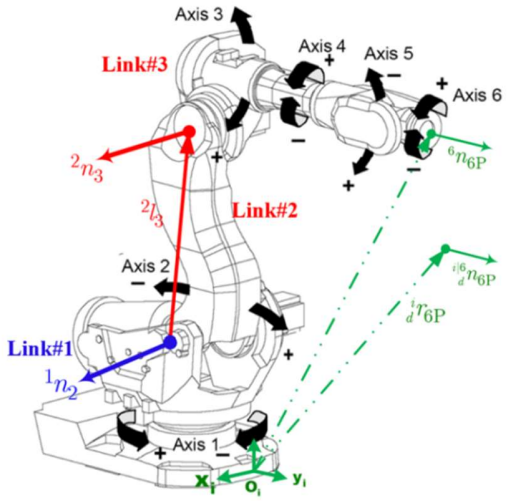

Fig. 1. Robot Arm Symbol Specification

The basic notation is as follows:

1) Lowercase letters with upper-left and lower-right corners indicate coordinate vectors, where: the upper-left indicator indicates the reference system, and for position vectors also the origin of the reference system.
2) Capital letters with upper-left and lower-right corners indicate coordinate matrices.
3) Lower case letters with upper and lower right corner labels stand for scalars.
4) Any coordinate vector defaults to a column vector.
5) The predecessor of k is written as $\overline{k}$, and predecessor of $\overline{k}$ is written as $\overline{\overline{k}}$.
6) The ${}^{\overline{k}}l_{k}$ stands for constant **l**ocation of Link# k with respect to Link# $\overline{k}$.

III. RECONCEPTUALIZING FIXED-AXIS ROTATION

Given a joint ${}^{\overline{l}}\mathrm{JT}_{l}$ between parent Link# $\overline{l}$ and child Link # l, its angular position by unit axis vector ${}^{\overline{l}}n_{l}$ is noted as $\phi_{l}^{\overline{l}}$. Clearly

$$\phi_{l}^{\overline{l}} = -\phi_{\overline{l}}^{l} \tag{4}$$

As shown in Fig. 2, the 1st-order screw of ${}^{l}r_{lS}$ is ${}^{\overline{l}}\tilde{n}_{l}\cdot{}^{l}r_{lS}$, and the 2nd-order screw of ${}^{l}r_{lS}$ is ${}^{\overline{l}}\tilde{n}_{l}^{\wedge 2}\cdot{}^{l}r_{lS}$, where $\wedge$ stands for power notation or separator.

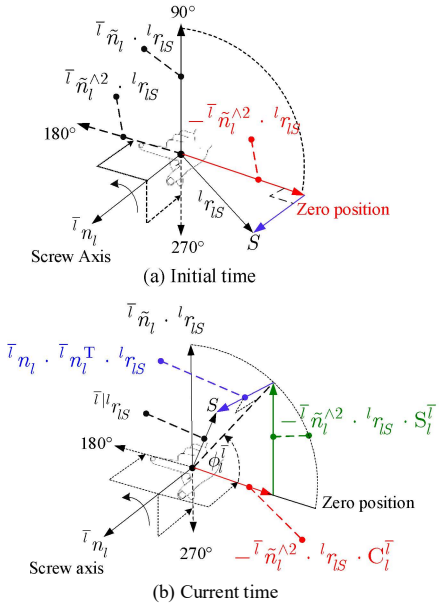

Fig. 2. Fixed axis rotation

Obviously

$$\begin{aligned} -{}^{\overline{l}}\tilde{n}_{l}\cdot{}^{l}r_{lS} &= {}^{\overline{l}}\tilde{n}_{l}^{\wedge 3}\cdot{}^{l}r_{lS} \\ -{}^{\overline{l}}\tilde{n}_{l}^{\wedge 2}\cdot{}^{l}r_{lS} &= {}^{\overline{l}}\tilde{n}_{l}^{\wedge 4}\cdot{}^{l}r_{lS} \end{aligned} \tag{5}$$

And

$${}^{l}r_{lS} - {}^{\overline{l}}\tilde{n}_{l}^{\wedge 2}\cdot{}^{l}r_{lS} = {}^{\overline{l}}n_{l}\cdot{}^{\overline{l}}n_{l}^{\mathrm{T}}\cdot{}^{l}r_{lS} \tag{6}$$

From Eq.(6)

$$-{}^{\overline{l}}\tilde{n}_{l}^{\wedge 2} = \mathbf{1} - {}^{\overline{l}}n_{l}\cdot{}^{\overline{l}}n_{l}^{\mathrm{T}} \tag{7}$$

Where **1** stands for unit matrix with size 3 by 3. From above, an axis vector and its screw matrix perform orthogonal projections. Let

$$\mathrm{C}_{l}^{\overline{l}} = \cos(\phi_{l}^{\overline{l}}),\ \mathrm{S}_{l}^{\overline{l}} = \sin(\phi_{l}^{\overline{l}}).$$

The vector ${}^{l}r_{lS}$ After rotating $\phi_{l}^{\overline{l}}$ radian along the axis direction ${}^{\overline{l}}n_{l}$, the vector is **orthogonally decomposed** into its axial, 1st order radial and zero-position direction components. Combining these components, we get

$$\left({}^{\bar{l}}n_l \cdot {}^{\bar{l}}n_l^{\mathrm{T}} + {}^{\bar{l}}\tilde{n}_l \cdot \mathrm{S}_l^{\bar{l}} - {}^{\bar{l}}\tilde{n}_l^{\wedge 2} \cdot \mathrm{C}_l^{\bar{l}}\right) \cdot {}^{l}r_{lS} = {}^{\bar{l}}Q_l \cdot {}^{l}r_{lS} \tag{8}$$

Where

$${}^{\bar{l}|l}r_{lS} = {}^{\bar{l}}Q_l \cdot {}^{l}r_{lS} \tag{9}$$

Where the bar | denotes orthogonal projection. The DCM ${}^{\bar{l}}Q_l$ stands for rotation from right frame to left frame, also for corresponds to orthogonal projection of left vector to right frame. Because ${}^{l}r_{lS}$ is an arbitrary vector, we obtain the following Rodrigues' rotation formula

$${}^{\bar{l}}Q_l = {}^{\bar{l}}n_l \cdot {}^{\bar{l}}n_l^{\mathrm{T}} + {}^{\bar{l}}\tilde{n}_l \cdot \mathrm{S}_l^{\bar{l}} - {}^{\bar{l}}\tilde{n}_l^{\wedge 2} \cdot \mathrm{C}_l^{\bar{l}} \tag{10}$$

Considering Eq.(10) and (7), obtain the DCM in terms of natural axis and angular position

$${}^{\bar{l}}Q_l = \mathbf{1} + {}^{\bar{l}}\tilde{n}_l \cdot \mathrm{S}_l^{\bar{l}} + {}^{\bar{l}}\tilde{n}_l^{\wedge 2} \cdot \left(1 - \mathrm{C}_l^{\bar{l}}\right) \tag{11}$$

Its inverse matrix is obtained by exchanging the upper left and lower right corner labels at the same time. Using Eq.(11), we have its Axis Vector

$$\mathrm{Vector}\left({}^{\bar{l}}Q_l\right) = {}^{\bar{l}}n_l \tag{12}$$

and

$${}^{l}n_{\bar{l}} \triangleq {}^{l|\bar{l}}n_l = {}^{l}Q_{\bar{l}} \cdot {}^{\bar{l}}n_l = \left(\mathbf{1} - {}^{\bar{l}}\tilde{n}_l \cdot \mathrm{S}_l^{\bar{l}} + {}^{\bar{l}}\tilde{n}_l^{\wedge 2} \cdot \left(1 - \mathrm{C}_l^{\bar{l}}\right)\right) \cdot {}^{\bar{l}}n_l = 1 \cdot {}^{\bar{l}}n_l$$

i.e.

$${}^{l}n_{\bar{l}} = {}^{\bar{l}}n_l \tag{13}$$

Eq.(13) says the axis vector, which has the same coordinate with respect to relative to its neighbouring frames, is an eigenvector and the scalar 1 is eigenvalue. Returning to Fig 1, the ${}^{\bar{l}}n_l$ is the common unit axis vector between Frames# $\bar{l}$ and # l. This is the reason for the use of n to denote full-order connection. One keenly discovers that this zero-axis is none other than the real axis of quaternions. Given a rotational chain in Fig. 1, its recursive position equation is shown as

$${}^{i}l_1 + {}^{0}Q_1 \cdot \left({}^{1}l_2 + {}^{1}Q_2 \cdot \left({}^{2}l_3 + {}^{2}Q_3 \cdot \left({}^{3}l_4 + {}^{3}Q_4 \cdot \left({}^{4}l_5 + {}^{5}Q_6 \cdot {}^{6}l_{6\mathrm{TCP}}\right)\right)\right)\right) = {}^{i}_{d}r_{6\mathrm{TCP}} \tag{14}$$

In Eq.(11), the motion of Link# l leads to its successors' motion. Using Eq.(9) and (14), the iterative position equation follows

$${}^{i}l_1 + {}^{i|1}l_2 + {}^{i|2}l_3 + {}^{i|3}l_4 + {}^{i|4}l_5 + {}^{i|5}l_{6\mathrm{TCP}} = {}^{i}_{d}r_{6\mathrm{TCP}} \tag{15}$$

Also using Eq.(11), get

$${}^{\bar{l}}_{0}Q_l = \mathbf{1} \quad if \quad \phi_l^{\bar{l}} = 0 \tag{16}$$

Eq.(16) says that Frames# $\bar{l}$ and # l have the same orientation in zero position. So, a coordinate system that has the same orientation at zero position is referred to as a **Natural Coordinate System**, which is used through this paper. The whole form $\left[{}^{\bar{l}}l_l, {}^{\bar{l}}n_l\right]$ composed of 3D position ${}^{\bar{l}}l_l$ and 3D direction ${}^{\bar{l}}n_l$ of axis# l is called fixed invariant.

IV. MEASURING THEORY OF STRUCTURAL PARAMETERS

During the measurement of structural parameters, only one joint moves at any one time, and the angular positions of other joints are kept constant. As shown in Fig. 3, the positions of the two Spherically Mounted Retro reflectors (SMR) S_0 and S_1' are recorded as and respectively at the initial time t_0.

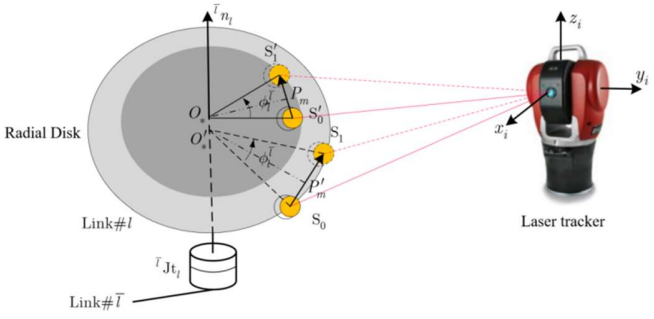

Fig. 3. Fig. 3 Laser tracker measure two SMRs fixed to the end-effector

The positions ${}^{i}r_{\mathrm{S}1}$ and ${}^{i}r_{\mathrm{S}'1}$ of SMRs and are recorded as and respectively at t_1. Therefore, the two radial vectors ${}^{i}r_{\mathrm{S}1} - {}^{i}r_{\mathrm{S}0}$ and ${}^{i}r_{\mathrm{S}'1} - {}^{i}r_{\mathrm{S}'0}$ are obtained to rotate around the axis vector ${}^{\bar{l}}n_l$. Taking the laser tracker frame as the world Frame # i for the measurement of the structural parameters, the accumulated error of the structural parameters can be reduced. Meanwhile, the laser tracker position measurement accuracy is usually better than 0.02 mm, and when the radial vector distance of the tracking ball is greater than 1,000 mm, the relative error of the joint position can be better than 2×10^-5Rad, about 3.8".

A. Measuring theory of axis direction vectors

Assuming ${}^{i}r_{\mathrm{S}0} - {}^{i}r_{\mathrm{S}'0} \neq 0_3$, ${}^{i}r_{\mathrm{S}1} - {}^{i}r_{\mathrm{S}'1} \neq 0_3$, obviously ${}^{i}r_{\mathrm{S}1} - {}^{i}r_{\mathrm{S}0}$ is not parallel to ${}^{\bar{l}}n_l$, obtain

$${}^{\bar{l}}n_l = \frac{\left({}^{i}r_{\mathrm{S}'1} - {}^{i}r_{\mathrm{S}'0}\right) \times \left({}^{i}r_{\mathrm{S}1} - {}^{i}r_{\mathrm{S}0}\right)}{\left\|{}^{i}r_{\mathrm{S}'1} - {}^{i}r_{\mathrm{S}'0}\right\| \cdot \left\|{}^{i}r_{\mathrm{S}1} - {}^{i}r_{\mathrm{S}0}\right\|} \tag{17}$$

B. Measuring theory of axis position vectors

The middle points of ${}^{i}r_{\mathrm{S}1} - {}^{i}r_{\mathrm{S}0}$ and ${}^{i}r_{\mathrm{S}'1} - {}^{i}r_{\mathrm{S}'0}$ are expressed respectively as

$$P_m = \begin{bmatrix} x_m \\ y_m \\ z_m \end{bmatrix} = \frac{{}^{i}r_{\mathrm{S}1} + {}^{i}r_{\mathrm{S}0}}{2} \tag{18}$$

and

$$P'_m = \begin{bmatrix} x'_m \\ y'_m \\ z'_m \end{bmatrix} = \frac{{}^{i}r_{\mathrm{S}'1} + {}^{i}r_{\mathrm{S}'0}}{2} \tag{19}$$

And obtain the coordinate vectors of $\overrightarrow{P_m O_*}$ and $\overrightarrow{P'_m O'_*}$

$$\begin{aligned} {}^{\overline{l}}k_l &= \begin{bmatrix} k_x \\ k_y \\ k_z \end{bmatrix} = \frac{{}^{\overline{l}}\tilde{n}_l \cdot \left({}^{i}r_{\mathrm{S}1} - {}^{i}r_{\mathrm{S}0} \right)}{\left\| {}^{\overline{l}}\tilde{n}_l \cdot \left({}^{i}r_{\mathrm{S}1} - {}^{i}r_{\mathrm{S}0} \right) \right\|} \\ {}^{\overline{l}}k'_l &= \begin{bmatrix} k'_x \\ k'_y \\ k'_z \end{bmatrix} = \frac{{}^{\overline{l}}\tilde{n}_l \cdot \left({}^{i}r_{\mathrm{S}'1} - {}^{i}r_{\mathrm{S}'0} \right)}{\left\| {}^{\overline{l}}\tilde{n}_l \cdot \left({}^{i}r_{\mathrm{S}'1} - {}^{i}r_{\mathrm{S}'0} \right) \right\|} \end{aligned} \tag{20}$$

Using Eq.(18) to (20), we can obtain the linear equation from the rotational centers O_* to P_m and the linear equation from the rotational centers O'_* to P'_m as follows

$$\begin{aligned} {}^{i}r_* &= \begin{bmatrix} x_* \\ y_* \\ z_* \end{bmatrix} = \begin{bmatrix} k_x \\ k_y \\ k_z \end{bmatrix} \cdot c_* + \begin{bmatrix} x_m \\ y_m \\ z_m \end{bmatrix} \\ {}^{i}r'_* &= \begin{bmatrix} x'_* \\ y'_* \\ z'_* \end{bmatrix} = \begin{bmatrix} k'_x \\ k'_y \\ k'_z \end{bmatrix} \cdot c'_* + \begin{bmatrix} x'_m \\ y'_m \\ z'_m \end{bmatrix} \end{aligned} \tag{21}$$

Where c_* and c'_* are linear parameters. Using Eq.(21), obtain the relative position from O_* to O'_*

$$\begin{bmatrix} x_* \\ y_* \\ z_* \end{bmatrix} - \begin{bmatrix} x'_* \\ y'_* \\ z'_* \end{bmatrix} = \begin{bmatrix} k_x & -k'_x \\ k_y & -k'_y \\ k_z & -k'_z \end{bmatrix} \cdot \begin{bmatrix} c_* \\ c'_* \end{bmatrix} + \begin{bmatrix} x_m - x'_m \\ y_m - y'_m \\ z_m - z'_m \end{bmatrix} \tag{22}$$

Considering the relative position vectors from the rotational centers $\left[x_* - x'_*, \quad y_* - y'_*, \quad z_* - z'_* \right]$ are parallel to the axis vector ${}^{\overline{l}}n_l$, we have

$$\begin{aligned} {}^{\overline{l}}\tilde{n}_l \cdot \begin{bmatrix} x_* - x'_* \\ y_* - y'_* \\ z_* - z'_* \end{bmatrix} &= {}^{\overline{l}}\tilde{n}_l \cdot \begin{bmatrix} k_x & -k'_x \\ k_y & -k'_y \\ k_z & -k'_z \end{bmatrix} \cdot \begin{bmatrix} c_* \\ c'_* \end{bmatrix} \\ + {}^{\overline{l}}\tilde{n}_l \cdot \begin{bmatrix} x_m - x'_m \\ y_m - y'_m \\ z_m - z'_m \end{bmatrix} &= 0_3 \end{aligned} \tag{23}$$

Which can be represented as

$${}^{\overline{l}}\tilde{n}_l \cdot \begin{bmatrix} k_x & -k'_x \\ k_y & -k'_y \\ k_z & -k'_z \end{bmatrix} \cdot \begin{bmatrix} c_* \\ c'_* \end{bmatrix} = {}^{\overline{l}}\tilde{n}_l \cdot \begin{bmatrix} x'_m - x_m \\ y'_m - y_m \\ z'_m - z_m \end{bmatrix} \tag{24}$$

Thus, by evaluating the above equation, we obtain:

$${}_3\mathrm{A}_2 \triangleq {}^{\overline{l}}\tilde{n}_l \cdot \begin{bmatrix} k_x & -k'_x \\ k_y & -k'_y \\ k_z & -k'_z \end{bmatrix} \tag{25}$$

Thus

$${}_3\mathrm{A}_2 \cdot \begin{bmatrix} c_* \\ c'_* \end{bmatrix} = {}^{\overline{l}}\tilde{n}_l \cdot \begin{bmatrix} x'_m - x_m \\ y'_m - y_m \\ z'_m - z_m \end{bmatrix} \tag{26}$$

The equation is composed of two independent radial vectors, making ${}_3\mathrm{A}_2^{\mathrm{T}} \cdot {}_3\mathrm{A}_2$ invertible. By solving the equation, we obtain the parameters for the two rows.

$$\begin{bmatrix} c_* \\ c'_* \end{bmatrix} = \left({}_3\mathrm{A}_2^{\mathrm{T}} \cdot {}_3\mathrm{A}_2 \right)^{-1} \cdot {}_3\mathrm{A}_2^{\mathrm{T}} \cdot {}^{\overline{l}}\tilde{n}_l \cdot \begin{bmatrix} x'_m - x_m \\ y'_m - y_m \\ z'_m - z_m \end{bmatrix} \tag{27}$$

Substituting the equation into another, we can derive the positions of the two rotation centers O_* and O'_*. Since the origin of the natural coordinate system lies on the axis line, we let the endpoint of position vector ${}^{\overline{l}}l_l$ to be the midpoint of the rotation center O_* and O'_*, from this, we obtain:

$$\begin{aligned} 2 \cdot {}^{\overline{l}}l_l &\triangleq \begin{bmatrix} x_* \\ y_* \\ z_* \end{bmatrix} + \begin{bmatrix} x'_* \\ y'_* \\ z'_* \end{bmatrix} \\ &= \begin{bmatrix} x_m \\ y_m \\ z_m \end{bmatrix} + \begin{bmatrix} x'_m \\ y'_m \\ z'_m \end{bmatrix} + \begin{bmatrix} k_x \\ k_y \\ k_z \end{bmatrix} \cdot c_* + \begin{bmatrix} k'_x \\ k'_y \\ k'_z \end{bmatrix} \cdot c'_* \end{aligned} \tag{28}$$

C. Measuring theory of joint angular positions

Let the initial radial vectors of the two tracking balls be

$${}^{i|\mathrm{S}0}r_* \triangleq \begin{bmatrix} k_x \\ k_y \\ k_z \end{bmatrix} \cdot l_* + 0.5 \cdot \left({}^{i}r_{\mathrm{S}1} - {}^{i}r_{\mathrm{S}0} \right) \tag{29}$$

$$ {}^{i|\mathrm{S0}}r'_{*} \triangleq \begin{bmatrix} k'_x \\ k'_y \\ k'_z \end{bmatrix} \cdot l' + 0.5 \cdot \left({}^{i}r_{\mathrm{S}'1} - {}^{i}r_{\mathrm{S}'0} \right) \tag{30} $$

From Fig.1 and Eq.(29) to (30), we derive

$$ \begin{aligned} {}_1\phi_l^{\bar{l}} &= \sin^{-1}\left(\frac{ {}^{\bar{l}}n_l^{\mathrm{T}} \cdot {}^{i|\mathrm{S0}}\tilde{r}_{*} \cdot {}^{\bar{l}}k_l }{ \left\| {}^{i|\mathrm{S0}}r_{*} \right\| } \right) \\ &+ \sin^{-1}\left(\frac{ {}^{\bar{l}}n_l^{\mathrm{T}} \cdot {}^{i|\mathrm{S0}}\tilde{r}'_{*} \cdot {}^{\bar{l}}k'_l }{ \left\| {}^{i|\mathrm{S0}}r'_{*} \right\| } \right) \end{aligned} \tag{31} $$

V. From Axis Invariants to D-H Parameters

As shown in Fig. 4, the natural coordinate system of Link# l is noted as Frame# l , and its corresponding DH system is noted as Frame# l' .

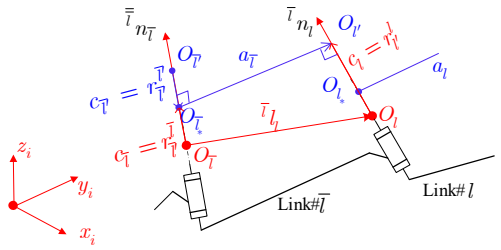

Fig.4 Relation between axis invariant and D-H parameters

Vector $^{\bar{l}}l_l$ point outward from the origin $O_{\bar{l}}$, ensuring the polarity of $x_{\bar{l}}$ remain consistent with $^{\bar{l}}l_l$, thus guaranteeing the uniqueness of the uniqueness of the DH system. The midpoint $O_{\bar{l}_*}$ and the origin $O_{l'}$ of Frame# l' are determined from the perpendicular bisector. Therefore, it's essential to characterize the positions of these two points using fixed axis vectors. Given the fixed axis invariants $\left[{}^{\bar{l}}l_{\bar{l}}, {}^{\bar{l}}n_{\bar{l}} \right]$ and $\left[{}^{\bar{l}}l_l, {}^{\bar{l}}n_l \right]$, compute the intersection points of the two axis lines with their common perpendicular.

$$ \begin{cases} {}^{\bar{l}}r_{\bar{l}} = {}^{\bar{l}}l_{\bar{l}} + c_{\bar{l}} \cdot {}^{\bar{l}}n_{\bar{l}} \\ {}^{\bar{l}}r_{l'} = {}^{\bar{l}}l_l + c'_l \cdot {}^{\bar{l}}n_l \end{cases} \tag{32} $$

The unit direction of the common normal $x_{\bar{l}}$ is give by

$$ {}^{\bar{l}}u_l = \frac{ {}^{\bar{l}}\tilde{n}_{\bar{l}} \cdot {}^{\bar{l}}n_l }{ \left\| {}^{\bar{l}}\tilde{n}_{\bar{l}} \cdot {}^{\bar{l}}n_l \right\| } \tag{33} $$

Hence, Twist Angular $\alpha_{\bar{l}} \in (-\pi, \pi)$ is written as

$$ \alpha_{\bar{l}} = 2 \cdot \sin^{-1}\left(\frac{ \left\| {}^{\bar{l}}\tilde{n}_{\bar{l}} \cdot {}^{\bar{l}}n_l \right\| }{ \mathrm{Sign}\left(\mathrm{C}_{lz}^{\bar{l}z} \right) \cdot \sqrt{2 + 2 \cdot \left\| \mathrm{C}_{lz}^{\bar{l}z} \right\|} } \right) \tag{34} $$

Where

$$ \mathrm{C}_{lz}^{\bar{l}z} = {}^{\bar{l}}n_{\bar{l}}^{\mathrm{T}} \cdot {}^{\bar{l}}n_l \tag{35} $$

Because the common normal is orthogonal to both axis lines, we have:

$$ \begin{cases} {}^{\bar{l}}\tilde{u}_l \cdot {}^{\bar{l}}r_{\bar{l}} = {}^{\bar{l}}\tilde{u}_l \cdot \left({}^{\bar{l}}l_{\bar{l}} + c_{\bar{l}} \cdot {}^{\bar{l}}n_{\bar{l}} \right) = 0 \\ {}^{\bar{l}}\tilde{u}_l \cdot {}^{\bar{l}}r_{l'} = {}^{\bar{l}}\tilde{u}_l \cdot \left({}^{\bar{l}}l_l + c'_l \cdot {}^{\bar{l}}n_l \right) = 0 \end{cases} \tag{36} $$

Where $c_{\bar{l}}$ and c'_l are scalar parameters for the lines, implying

$$ \begin{cases} c_{\bar{l}} \cdot {}^{\bar{l}}\tilde{u}_l \cdot {}^{\bar{l}}n_{\bar{l}} = -{}^{\bar{l}}\tilde{u}_l \cdot {}^{\bar{l}}l_{\bar{l}} \\ c'_l \cdot {}^{\bar{l}}\tilde{u}_l \cdot {}^{\bar{l}}n_l = -{}^{\bar{l}}\tilde{u}_l \cdot {}^{\bar{l}}l_l \end{cases} \tag{37} $$

Thus

$$ {}_3\mathrm{A}_2 \cdot \begin{bmatrix} c_{\bar{l}} \\ c'_l \end{bmatrix} = {}^{\bar{l}}\tilde{u}_l \cdot {}^{\bar{l}}l_l - {}^{\bar{l}}\tilde{u}_l \cdot {}^{\bar{l}}l_{\bar{l}} \tag{38} $$

Where

$$ {}_3\mathrm{A}_2 = \begin{bmatrix} {}^{\bar{l}}\tilde{u}_l \cdot {}^{\bar{l}}n_{\bar{l}}, & -{}^{\bar{l}}\tilde{u}_l \cdot {}^{\bar{l}}n_l \end{bmatrix} \tag{39} $$

When the two axes are not parallel, solving the equation yields the Offset Distance as:

$$ \begin{aligned} \begin{bmatrix} c_{\bar{l}} \\ c'_l \end{bmatrix} &= \left({}_3\mathrm{A}_2^{\mathrm{T}} \cdot {}_3\mathrm{A}_2 \right)^{-1} \cdot {}_3\mathrm{A}_2^{\mathrm{T}} \\ &\cdot \left({}^{\bar{l}}\tilde{u}_l \cdot {}^{\bar{l}}l_l - {}^{\bar{l}}\tilde{u}_l \cdot {}^{\bar{l}}l_{\bar{l}} \right) \end{aligned} \tag{40} $$

Clearly, we have

$$ c_{\bar{l}} = c_{\bar{l}} - c'_{\bar{l}} \tag{41} $$

Substituting the result of the equation into another equation, Using Eq.(32), obtain common normal

$$ {}^{\bar{l}}r_{l'} - {}^{\bar{l}}r_{\bar{l}} = {}^{\bar{l}}l_l + c_l \cdot {}^{\bar{l}}n_l - {}^{\bar{l}}l_{\bar{l}} - c_{\bar{l}} \cdot {}^{\bar{l}}n_{\bar{l}} \tag{42} $$

We obtain Link Distance

$$ \begin{aligned} a_{\bar{l}} &= {}^{\bar{l}}u_l^{\mathrm{T}} \cdot \left({}^{\bar{l}}r_{l'} - {}^{\bar{l}}r_{\bar{l}} \right) \\ &= {}^{\bar{l}}u_l^{\mathrm{T}} \cdot \left({}^{\bar{l}}l_l + c_l \cdot {}^{\bar{l}}n_l - {}^{\bar{l}}l_{\bar{l}} - c_{\bar{l}} \cdot {}^{\bar{l}}n_{\bar{l}} \right) \end{aligned} \tag{43} $$

Initial joint angular ${}_0\phi_l \in (-\pi, \pi)$ is expressed as

$$ {}_0\phi_l = 2 \cdot \sin^{-1}\left(\frac{ \left\| {}^{\bar{l}}\tilde{u}_{\bar{l}} \cdot {}^{\bar{l}}u_l \right\| }{ \mathrm{Sign}\left(\mathrm{C}_{lx}^{\bar{l}x} \right) \cdot \sqrt{2 + 2 \cdot \left\| \mathrm{C}_{lx}^{\bar{l}x} \right\|} } \right) \tag{44} $$

Where

$$ \mathrm{C}_{lx}^{\bar{l}x} = {}^{\bar{l}}u_{\bar{l}}^{\mathrm{T}} \cdot {}^{\bar{l}}u_l \tag{45} $$

VI. Verification of Method

Based on the above principle, C++ was applied to develop the software for measuring the structural parameters of the robot. The test platform, shown in Fig. 5, consists of the robot under

test, the laser tracker and the structural parameter measurement system. Examples of tests are shown in Table 1 and 2. After applying the new structural parameters, the absolute positioning accuracy of the robot under test is improved from 1.5 mm to 0.3 mm. experiments show the correctness and applicability of the above principle.

Fig.5 Test bed of robot structure parameters

TABLE I. AXIS INVARIANT

Axis No	Joint Axis Position (m)	Joint Axis Direction	Common normal
1	[0.0000, 0.0000, 0.0000]	[0.0000, 0.0000, 1.0000]	[1.0000, 0.0000, 0.0000]
2	[0.0000, -0.2080, 1.3000]	[0.0000, -1.0000, 0.0000]	[-0.0100, 0.0000, 0.9999]
3	[0.0090, 0.2079, 0.4001]	[0.9999, -0.0100, 0.0100]	[-0.0100, -1.0000, 0.0000]
4	[-0.0090, 0.0001, 0.8999]	[0.0000, 0.0000, 1.0000]	[1.0000, -0.0100, 0.0000]
5	[-0.0021, -0.2080, -0.200]	[-0.0100, -1.0000, 0.000]	[-0.0100, 0.0001, 1.0000]
6	[0.8655, 0.1914, 0.0086]	[0.9999, -0.0100, 0.0100]	[0.0139, 0.5596, -0.8287]

TABLE II. D-H PARAMETERS

Axis No	Initial joint angular (Deg)	Twist angular (Deg)	Offset distance (m)	Link distance (m)
1	0.00000	90.00000	0.00000	1.30000
2	90.57297	89.42709	-0.89995	-0.20790
3	89.99427	89.42706	0.20798	-0.01592
4	90.00000	90.00000	0.00900	-0.59993
5	90.57294	90.00000	0.19999	-0.20000
6	0.00000	0.00000	0.00000	0.00000

VII. CONCLUSION

This paper introduces an enhanced methodology for measuring robot structural parameters using axis invariants. We have redefined fixed-axis rotation and axis invariants, followed by the implementation of a laser tracker to measure the positions of two tracking balls attached to the robot end. This setup aids in determining joint axis directions, positions, angle positions, and line positions. Subsequently, these measurements are utilized to ascertain the robot's DH parameters. Our theoretical analysis, supported by experimental validation, underscores the effectiveness of this methodology in significantly enhancing the robot's absolute positioning accuracy.

REFERENCES

[1] R. P. Judd and A. B. Knasinski, ‘‘A technique to calibrate industrial robots with experimental verification,’’ IEEE Trans. Robot. Autom., vol. 6, no. 1, pp. 20–30, Mar. 1987.

[2] A. Y. Elatta, P. G. Li, F. L. Zhi, and D. Yu, ‘‘An overview of robot calibration,’’ Inf. Technol. J., vol. 3, no. 1, pp. 377–385, 2004.

[3] F. Leali, A. Vergnano, F. Pini, M. Pellicciari, and G. Berselli, ‘‘A workcell calibration method for enhancing accuracy in robot machining of aerospace parts,’’ Int. J. Adv. Manuf. Technol., vol. 85, nos. 1–4, pp. 47–55, Jul. 2016.

[4] L. Ma, P. Bazzoli, P. M. Sammons, R. G. Landers, and D. A. Bristow, ‘‘Modeling and calibration of high-order joint-dependent kinematic errors for industrial robots,’’ Robot. Comput.-Integr. Manuf., vol. 50, pp. 153–167, Apr. 2018.

[5] H. Wang, X. Lu, Z. Hu, and Y. Li, ‘‘A vision-based fully-automatic calibration method for hand-eye serial robot,’’ Ind. Robot, Int. J., vol. 42, no. 1, pp. 64–73, Jan. 2015.

[6] S. He, L. Ma, C. Yan, C.-H. Lee, and P. Hu, ‘‘Multiple location constraints based industrial robot kinematic parameter calibration and accuracy assessment,’’ Int. J. Adv. Manuf. Technol., vol. 102, nos. 5–8, pp. 1037–1050, 2018.

[7] D. Wu, ‘‘Novel approach to calibrate main body of a three-dimensional scanning robotic system,’’ J. Mech. Eng., vol. 47, no. 17, p. 9, 2011.

[8] G. Chen, Q. Jia, T. Li, and H. Sun, ‘‘Calibration method and experiments of robot kinematics parameters based on error model,’’ Robot, vol. 34, no. 6, p. 680, 2012.

[9] X. Zhang, Y. Song, Y. Yang, and H. Pan, ‘‘Stereo vision based autonomous robot calibration,’’ Robot. Auto. Syst., vol. 93, pp. 43–51, Jul. 2017.

[10] M. Gaudreault, A. Joubair, and I. Bonev, ‘‘Self-calibration of an industrial robot using a novel affordable 3D measuring device,’’ Sensors, vol. 18, no. 10, p. 3380, Oct. 2018. [11] J.-M. Renders, E. Rossignol, M. Becquet, and R. Hanus, ‘‘Kinematic calibration and geometrical parameter identification for robots,’’ IEEE Trans. Robot. Autom., vol. 7, no. 6, pp. 721–732, Dec. 1991.

[12] A. Filion, A. Joubair, A. S. Tahan, and I. A. Bonev, ‘‘Robot calibration using a portable photogrammetry system,’’ Robot. Comput.-Integr. Manuf., vol. 49, pp. 77–87, Feb. 2018. [13] P. Yang, Z. Guo, and Y. Kong, ‘‘Plane kinematic calibration method for industrial robot based on dynamic measurement of double ball bar,’’ Precis. Eng.-J. Int. Soc. Precis. Eng. Nanotechnol., vol. 62, pp. 265–272, Mar. 2020.

[14] K. Schröer, S. L. Albright, and M. Grethlein, ‘‘Complete, minimal and model-continuous kinematic models for robot calibration,’’ Robot. Comput.-Integr. Manuf., vol. 13, no. 1, pp. 73–85, Mar. 1997.

[15] I.-M. Chen, G. Yang, C. T. Tan, and S. H. Yeo, ‘‘Local POE model for robot kinematic calibration,’’ Mechanism Mach. Theory, vol. 36, nos. 11–12, pp. 1215–1239, Nov. 2001. [16] M. Ish, ‘‘Kinematic model and calibration of a robot manipulator,’’ Adv. Robot., vol. 5, no. 3, pp. 337–347, 2010.

[17] I. C. Ha, ‘‘Kinematic parameter calibration method for industrial robot manipulator using the relative position,’’ J. Mech. Sci. Technol., vol. 22, no. 6, p. 1084, 2008.

[18] R. Wang, A. Wu, X. Chen, and J. Wang, ‘‘A point and distance constraint based 6R robot calibration method through machine vision,’’ Robot. Comput.-Integr. Manuf., vol. 65, Oct. 2020, Art. no. 101959.

[19] A. Nowrouzi, Y. B. Kavina, H. Kochekali, and R. A. Whitaker, ‘‘An overview of robot calibration techniques,’’ Ind. Robot, vol. 15, no. 4, pp. 229–232, 1988.

[20] M. R. Driels, W. Swayze, and S. Potter, ‘‘Full-pose calibration of a robot manipulator using a coordinate-measuring machine,’’ Int. J. Adv. Manuf. Technol., vol. 8, no. 1, pp. 34–41, Jan. 1993.

[21] A. Nubiola and I. A. Bonev, ‘‘Absolute calibration of an ABB IRB 1600 robot using a laser tracker,’’ Robot. Comput.-Integr. Manuf., vol. 29, no. 1, pp. 236–245, Feb. 2013. [22] A. Nubiola and I. A. Bonev, ‘‘Absolute robot calibration with a single telescoping ballbar,’’ Precis. Eng., vol. 38, no. 3, pp. 472–480, Jul. 2014.

[23] Y. Meng and H. Zhuang, ‘‘Autonomous robot calibration using vision technology,’’ Robot. Comput.-Integr. Manuf., vol. 23, no. 4, pp. 436–446, Aug. 2007.

[24] G. Du, P. Zhang, and D. Li, ‘‘Online robot calibration based on hybrid sensors using Kalman filters,’’ Robot. Comput.-Integr. Manuf., vol. 31, pp. 91–100, Feb. 2015.

[25] W. K. Veitschegger and C.-H. Wu, ‘‘Robot calibration and compensation,’’ in Proc. Int. Conf. Robot. Autom., 1988, vol. 4, no. 6, pp. 643–656.

[26] J. M. Renders, E. Rossignol, M. Becquet, and R. Hanus, ‘‘Kinematic calibration and geometrical parameter identification for robots,’’ in Proc. Int. Conf. Robot. Autom., 1991, vol. 7, no. 6, pp. 721–732.

[27] W. Khalil, M. Gautier, and C. Enguehard, ‘‘Identifiable Parameters and Optimum Configurations for Robots Calibration,’’ Robotica, vol. 9, no. 1, p. 63, 1991.

[28] S. Zhang, S. Wang, F. Jing, and M. Tan, ‘‘Parameter estimation survey for multi-joint robot dynamic calibration case study,’’ Sci. China Inf. Sci., vol. 62, no. 10, pp. 1–15, Oct. 2019.

[29] J. U. Dolinsky, I. D. Jenkinson, and G. J. Colquhoun, ‘‘Application of genetic programming to the calibration of industrial robots,’’ Comput. Ind., vol. 58, no. 3, pp. 255–264, Apr. 2007.

[30] P. Xiao et al, “New Fixed Axis-Invariant Based Calibration Approach to Improve Absolute Positioning Accuracy”, IEEE Access Vol. 8,pp**:** 134224 – 134232, 2020.

Authors’ background

Name	Prefix	Research Field	Email	Personal website
Yiran Ju		Robotics and computer engineering	juyiran@alumni.ubc.ca	
Yu Meng	Associate Professor	Robotics and computer engineering	yuxy21@nuaa.edu.cn	

Note:

[1] **This form helps us to understand your paper better; the form itself will not be published.**

[2] *Prefix***:** can be chosen from Master Student, PhD Candidate, Assistant Professor, Lecturer, Senior Lecturer, Associate Professor, Full Professor